tvst

Article

Subretinal Drusenoid Deposit Formation: Insights From Turing Patterns

Benjamin K. Young[1,2], Liangbo L. Shen[1], and Lucian V. Del Priore[1]

[1] Department of Ophthalmology and Visual Sciences, Yale University School of Medicine, New Haven, CT, USA
[2] Kellogg Eye Center, Department of Ophthalmology, University of Michigan Medical School, Ann Arbor, MI, USA

Correspondence: Lucian V. Del Priore, Robert R. Young Professor and Chair, Department of Ophthalmology and Visual Science, Yale University School of Medicine, 40 Temple Street, Suite 1B, New Haven, CT 06510, USA.
e-mail: lucian.delpriore@yale.edu

Received: March 31, 2021
Accepted: December 28, 2021
Published: March 7, 2022

Keywords: subretinal drusenoid deposits; macular degeneration; Turing patterns; computational simulation

Citation: Young BK, Shen LL, Del Priore LV. Subretinal drusenoid deposit formation: Insights from turing patterns. Transl Vis Sci Technol. 2022;11(3):5, https://doi.org/10.1167/tvst.11.3.5

Purpose: The purpose of this study was to demonstrate that the organized formation of subretinal drusenoid deposits (SDDs) may be a Turing pattern.

Methods: A Java-based computational model of an inferred reaction-diffusion system using paired partial differential equations was used to create topographic images. Reaction kinetics were varied to illustrate a spectrum of pattern development, which were then compared to dot-like, reticular, and confluent SDD patterns observed clinically.

Results: A reaction-diffusion system using two agents, one an "activator" that increases its own production, and the other an "inhibitor" that decreases the activator's production, can create patterns that match the spectrum of topographic appearance of organized SDD. By varying a single parameter, the strength of the activator, the full spectrum of clinically observed SDD patterns can be generated. A new pattern, confluence with holes, is predicted and identified in one case example.

Conclusions: The formation of clinically significant SDD and its different patterns can be explained using Turing patterns obtained by simulating a two-component reaction-diffusion system.

Translational Relevance: This model may be able to guide future risk stratification for patients with SDD, and provide mechanistic insights into the cause of the disease.

Introduction

Subretinal drusenoid deposits (SDDs), also referred to as reticular pseudodrusen, are present in some patients with age-related macular degeneration (AMD), Sorsby's macular dystrophy, and pseudoxanthoma elasticum.[1,2] They are distinct from drusen given their anatomic position above the retinal pigment epithelium (RPE), unlike the typical location of drusen underneath the RPE, as identified by optical coherence tomography (OCT).[3] Classically, SDDs show characteristic reticular patterns (i.e. net-like structures), but some patients exhibit multiple dot-like or confluent deposits. Moreover, many of these topographic patterns may be found in the same eye.

Several studies have demonstrated that the presence of SDD is an independent risk factor for the progression to both neovascular AMD and geographic atrophy (GA).[3–5] The specific cause and mechanisms of SDD have not yet been elucidated. There is evidence that complement activation may be involved, as mutations in complement factor H have been associated with the development of SDD in mouse models and possibly humans.[6,7] A detailed biogenesis model for the formation of SDD has also been proposed, with a complex interplay among unesterified cholesterol, high-density lipoprotein (HDL) particles, and RPE-photoreceptor cycling.[8] However, although biogenesis models of SDD have been proposed, it is not understood why they occur in distinct and characteristic geometric subretinal patterns.[8,9] A key concept is whether the geometric patterns that are observed arise from the geometry of adjacent structures, or whether these patterns can arise de novo. One hypothesis proposed that the organized reticular pattern of pseudodrusen

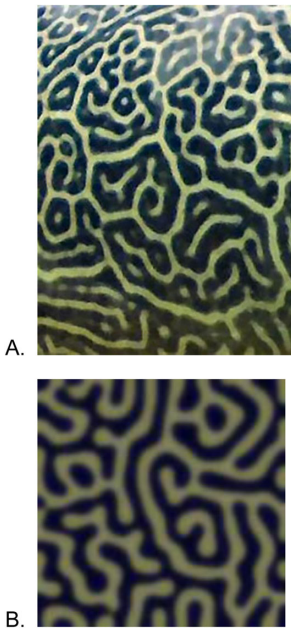

Figure 1. (**A**) Detail of skin pattern of a giant pufferfish, which bears resemblance to **B**. (**B**) A computational simulation for a simple reaction-diffusion system. Image: Chiswick Chap/Wikimedia Commons, used under Creative Commons license (CC BY-SA 3.0).[30]

develops due to the underlying pattern of the choroidal vessels.[10] However, a stereological study demonstrated that the patterning of choroidal vessels and SDD were independent of one another.[11] Others have suggested that these morphologies may be independent of the geometry of adjacent structures, but without further indication as to why highly organized morphological patterns develop in the subretinal space.[12]

In nature, complex patterns can emerge spontaneously due to physical and chemical forces that may not have an underlying pattern themselves. In 1952, mathematician Alan Turing proposed a framework to explain spontaneous complex pattern formations in nature.[13] In brief, a two-component system of interacting compounds can generate highly organized patterns if one compound is an activator and the second compound is an inhibitor of the activation reaction.[10] Prominent examples of Turing patterns in nature include the formation of stripes on zebras, spots on leopards, and the complex skin pattern of puffer fish (Fig. 1).[13,14] An experimental example of Turing pattern generation is in the hybridization of the white-spotted char fish, where a range of Turing patterns can be generated by breeding char with different skin patterns.[15] A prototypical example of a Turing pattern is a simplified predator-prey model involving rabbit and fox populations, where the rabbits (activators) increase their own population by breeding, and the foxes (inhibitors) decrease rabbit population by eating them (Fig. 2). Although this is an oversimplification of actual predator-prey dynamics, it is analogous to activators and inhibitors in a reaction-diffusion system to generate a Turing pattern from the distribution of the rabbit population. Turing inferred that, under the right conditions, stable and complex patterns can emerge in such systems. We propose that the morphologies seen in the formation of SDD in the subretinal space are examples of the formation of Turing patterns in this environment. This provides a uniform explanation for the spontaneous development of SDD patterns in the subretinal space and may account for the variation in the observed patterns seen in patients.

Methods

In a two-component system, we can represent the concentration of each molecule as "u" and "v."

$u = [Activator]$, or concentration of the activator
$v = [Inhibitor]$, or concentration of the inhibitor

The concentration of each compound will change as a function of time as well as position in the two-dimensional (2D) space due to diffusion; thus, we write[13]:

$$\frac{\delta \mathrm{u}}{\delta \mathrm{t}} = f(u, v) + D_u \nabla^2 \mathrm{u}$$
$$\frac{\delta \mathrm{v}}{\delta \mathrm{t}} = g(u, v) + D_v \nabla^2 \mathrm{v}$$

Where the Laplacian operator ∇^2, is defined in 2D space as:

$$\nabla^2 f = \frac{\delta^2 f}{\delta^2 x} + \frac{\delta^2 f}{\delta^2 y}$$

Where u and v are the concentrations of the diffusible activator and the inhibitor, respectively, f (u, v) and g (u, v) are functions that govern the reaction kinetics between u and v, D_u and D_v are diffusion coefficients for each compound, and ∇^2 is the Laplacian operator that captures the effects of a concentration gradient on spatial diffusion kinetics. For demonstrative purposes, a simple linear example is used; in this case, the reaction kinetic equations can be written in the following forms:

$$f(u, v) = Au - Bv$$
$$g(u, v) = Cu - Dv$$

Where f (u, v) describes the changes in production of activator "u" and g (u, v) describes the changes in production of inhibitor "v"; here, A, B, C, and D are constants governing reaction kinetics.

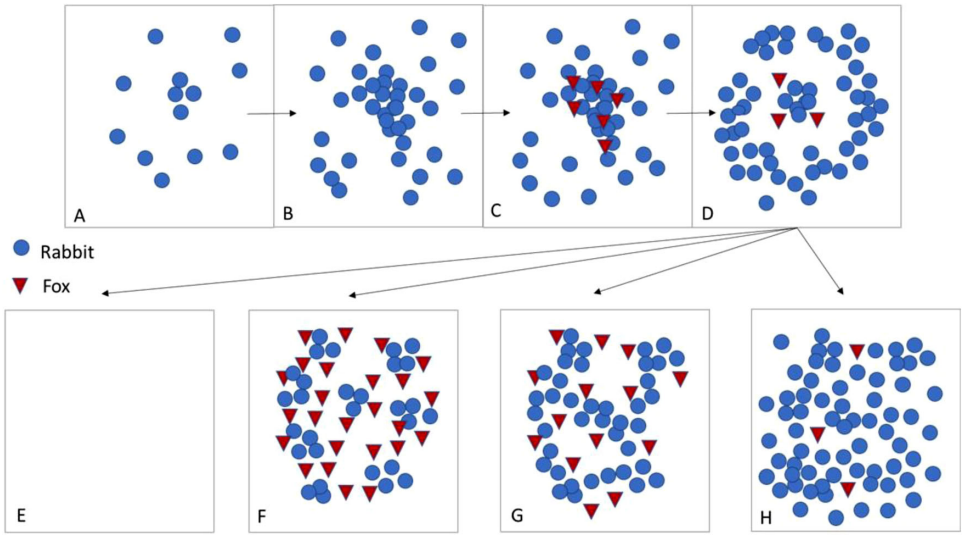

Figure 2. Schematic example of reaction-diffusion systems. *Blue circles* are "rabbits," which when in proximity, promote production of other rabbits. *Red triangles* are "foxes," which both decrease the local concentration of rabbits by eating them, but also decrease in population when rabbit populations decrease. (**A**) Rabbits are initially randomly distributed. (**B**) Where there are more rabbits, the local concentration of rabbits increases. (**C**) An increase in rabbits leads to an increase in the number of foxes due to the increase in the fox food supply. (**D**) An increase in foxes will decrease the local population of rabbits. Because foxes are faster than rabbits, they tend toward the edges of local concentrations or rabbits (i.e. foxes "diffuse" faster than rabbits). This process repeats, and, under the correct parameters, there are four possible stable equilibria (**E**). The foxes are too effective, and cause extinction among the rabbits (and, ultimately, their own extinction). (**F**) The foxes establish an equilibrium where pockets of rabbit populations are stable. (**G**) The foxes are less effective than in **F**, and they form stable reticulated networks of rabbit populations. These stable populations as in **F** and **G** that result from reaction-diffusion kinetics between at least two factors (**H**). The foxes are insufficiently effective, and the rabbit populations densely cover the area.

This series of equations is easiest understood using the rabbit-fox metaphor as an example (see Fig. 1); here, "u" refers to the population density of rabbits, and "v" the population density of foxes. The physical meaning of the terms of the above equations are then as follows:

- A*u is a term that captures the increase in rabbits as they reproduce, because the density of new rabbits depends upon the pre-existing rabbit density;
- B*v is a term that captures the loss of the rabbit density that are being eaten by the foxes;
- C*u is a term that captures the density of the fox population. Here, the rabbits are the food supply for the foxes, and thus the number of foxes will increase as the number of rabbits increases (not by the number of foxes); and
- D*v is a term that captures the decrease in the fox density that occurs due to natural death of the foxes. Here, the loss of density of the foxes or death of foxes is proportional to the number of foxes in the population.

Many programs have been developed to illustrate Turing patterns, using a reaction diffusion simulation. In this paper, we use a previously published Java-based simulation whose full details are available elsewhere.[5] This program creates an initial condition with initial noise and then uses the above differential equations to determine the behavior of reaction components u and v as a function of time. The default values used in this simulation were used for the purposes of this demonstration, where only the activating parameter "A" was varied to generate a range of possible Turing patterns.

For this demonstration, and to illustrate the effect of increasing the strength of the activator component on pattern formation, we allow parameter A to vary from 0.08 to 0.15 while we hold B, C, D, D_u, and D_v constant, at 0.06, 0.04, 0.07, 0, and -0.15, respectively. Our results were compared directly to the appearance described previously of confluent, reticular, and dot conformation pseudodrusen using images from a prior report, and plotted in comparison.[4]

This paper did not involve human subjects, human-derived materials, or human medical records.

Results

Figure 3A shows representative fundus photographs with SDD visualization enhanced by selecting the blue

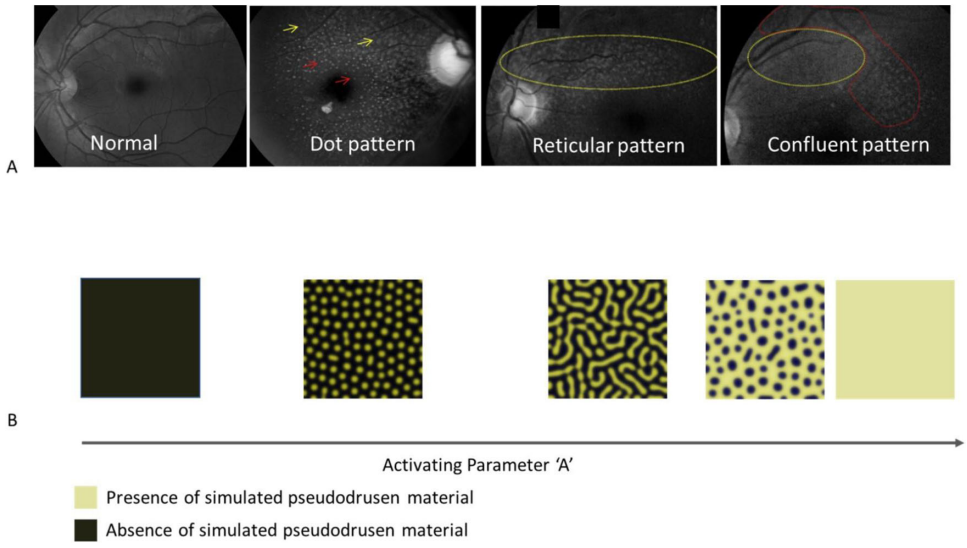

Figure 3. Subretinal drusenoid deposits (SDDs) morphology compared to Turing patterns generated with different values of A, which measures the strength of the activator effect.[4,14] Top images are representative fundus photographs enhanced by including only the blue channel, including a normal control, and with a spectrum of SDD morphology, as presented by Zhou et al. (figures reproduced with permission from the publisher).[4,31] *Bottom images* depict Turing patterns expected as we change A, a reaction kinetics parameter. *Yellow* indicates the presence of the activator, where *black* represents its absence.[5] By changing a single reaction kinetic parameter, all SDD morphologies can be generated. Note that in confluent SDD, small "holes" are observed in the SDD on close inspection, as predicted by the Turing pattern. Images are used with the explicit permission of the publisher.[4]

channel, as presented by Zhou et al.[4] Figure 3B images depict a Turing pattern that would form a theoretical component "u" as the value of A, the activation parameter is changed where yellow indicates the presence of the "u," and black represents its absence.[14] By changing the value of A, which measures the strength of the activator effect; we can generate all three morphologies for SDD.

In the rabbit-fox model we have used as an illustrative example (see Fig. 2), "A" represents the rabbit's effectiveness at procreation. As we increase the effect of A, or, in other words, the relative ability for rabbits to reproduce compared to the foxes' ability to eat them, there is a transition from no activator material to a dot pattern, reticular pattern, confluence with holes, and a full confluent pattern.

Note that this Turing pattern simulation predicts a morphology that would be a confluent pattern with holes not represented in previous studies; however, re-inspection of the representative confluent pattern shows the possible appearance of these "holes" within the confluent SDD (Fig. 4, orange inset). Furthermore, the full Turing pattern spectrum can be visualized in this image, from confluent to absence of pseudodrusen material, and the patterns appear in the order predicted by the Turing pattern simulation (see Fig. 4).

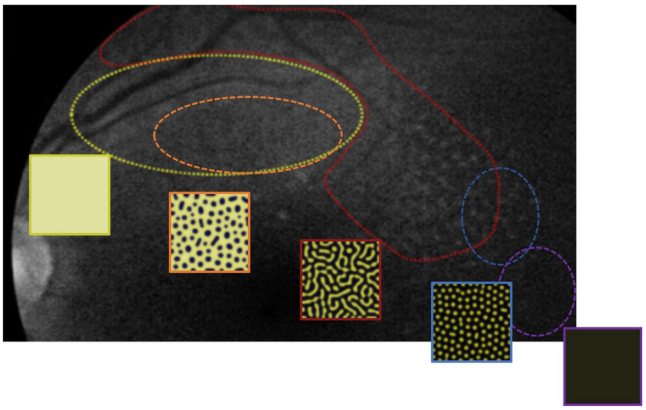

Figure 4. Zoomed in view of the "Confluent pattern" panel from Figure 3A, demonstrating that all Turing patterns can develop within one eye, and follows the same ordinal pattern as the Turing spectrum. The simulated pattern is shown in the *square box*, matched with the corresponding *colored encircled* area. *Yellow* – confluent pattern, *orange* – confluent with holes, *red* – reticular pattern, *blue* – dot pattern, and *purple* – no pattern. By combinatorics, the chance of this happening at random is 2/5!, or 1.7%.

Discussion

SDD can appear as several distinct patterns in the subretinal space, yet, to date, there is an incomplete

understanding of why these morphological patterns emerge.[8,12] These patterns have previously been characterized as confluent, reticular (i.e. ribbon-like or a network-like structure), or multiple dots. In this paper, we demonstrate a mechanism by which the morphological features seen in the distribution of SDD could arise spontaneously, without reliance on an underlying pattern of cells in the retina, RPE, or choroid. Thus, SDD development could be spontaneous Turing patterns arising from the presence of a yet unknown activator and inhibitor agents. In our model, Turing patterns that resemble the full spectrum of SDD morphology were simulated using only two partial differential equations with simple assumptions; namely, that an activator is present and that there is an inhibitor that decreases the amount of the activator.

No organized pattern is seen when the strength of the activator is too high or too low. A low value of A (i.e. activator strength) when other parameters, including strength of the inhibitor, are held constant implies that the activator effect will be overwhelmed by the inhibitor, and no pattern will develop. Similarly, a high level of A indicates that there is overwhelming activation, which would be consistent with a confluent buildup of subretinal drusenoid deposit, as seen in the confluent pattern (see Fig. 3). For intermediate values of reaction inhibition, our model generates the two other major morphological categories of SDD, dot and reticular.

Several additional pieces of evidence suggest that the spontaneous development of SDD morphology is an example of a Turing pattern. For example, SDDs tend to increase in anterior-posterior height over time, but not width.[3] This suggests an underlying 2D waveform driving SDD formation remains stable, even as more material accumulates in the subretinal space. This suggests that the pattern of SDD formation is an organized process over time, as opposed to a disorganized process, as may be the case in age-related accumulation of drusen in the sub-RPE space. Not all spots or deposits that arise in the subretinal or sub-RPE space would be expected to arise from Turing patterns, as not all "spots" that occur in the real world develop on this basis. Notably, other spots, such as drusen, do not show the high organization of reticular pseudodrusen or SDD, suggesting that drusen form by another, more random mechanism of spot formation. However, this analysis did not specifically analyze drusen.

It is important to note that different SDD patterns can be seen within the same retina. This implies that within the same patient, there can be significant regional topographic variation in inhibition of the formation of SDD. In one example from the literature, the full spectrum of the Turing pattern simulation can be seen in the same retina, with patterns arising in the same sequence predicted by the simulation (see Fig. 4). In addition, the balance between the activator and inhibitor changes with age, because SDDs accumulate in patients as a function of age and are seldom seen in young adults. This implies that the reaction parameters change with patient age, or that the SDD accumulation is very slow and gradual.

Our model demonstrates that a reaction-diffusion system may exist to drive SDD formation, which can provide other investigators an understanding of SDD patterns as occurring along a spectrum and organizing future study of SDD characteristics in this order. However, this model does not allow us to identity the specific molecular activator or inhibitor of SDD formation. The biogenesis model for SDD formation expounded upon by Curcio et al., based on histologic analysis of SDD, also does not have immediate suggestions for activator-inhibitor candidates.[8,9] Additional studies are required to identify the molecular basis of SDD formation in the subretinal space.

SDDs have been demonstrated to independently increase the risk ratio of developing advanced AMD, including both neovascular AMD and geographic atrophy.[3,4,16–19] Some activation-inhibition systems have been implicated previously as risk factors for the development of advanced AMD, including the complement system, which has careful regulation through activator-inhibitor feedback systems. For example, complement factor H, whose gene may predispose some patients to developing AMD, is an important inhibitor of the alternate complement pathway.[20] In mouse models, an absence of *CFH* leads to an organized accumulation of subretinal deposits in a dot-like conformation that appears to mimic some aspects of SDD in humans. Ultimately, this leads to significant downstream effects, including the upregulation of C3.[6] One study found variation in the distribution of CFH I62V polymorphisms between patients with dot-dominant and dot-reticular patterns (termed dot-ribbon, in this study).[7] However, there is conflict in the literature on whether this I62V polymorphism, and the Y402H variant, which is also associated with AMD, actually have higher prevalence in patients with subretinal drusenoid deposits.[21–24]

Another possibility that may fit this activator-inhibitor system involves the vitamin A and retinoid cycles, which have previously been suggested to drive SDD formation based on OCT findings.[12] Specifically, vitamin A deficiency can cause subretinal, organized reticular patterns.[25,26] A defect of retinoid metabolism includes retinitis punctata albescens, which is caused by a mutation in retinaldehyde binding protein 1

(RLBP1), and fundus albipunctatus can be caused by mutations in the gene for retinol dehydrogenase 5 (RDH5), which participates in 11-cis-retinal synthesis. Both diseases have characteristic, highly organized dot-like subretinal lesions, and, in some cases, peripheral reticular patterns.[27] Here, disruption of the production and consumption in the retinoid cycle of 11-cis retinal may serve as the activator-inhibitor roles that would result in Turing pattern formation. It is important to note that other diseases can exhibit SDD, including Sorsby's macular dystrophy and pseudoxanthoma elasticum.[2,28] The fact that SDD may occur in a range of diseases suggests that the mechanism causing SDD are generalized, and possibly not disease specific.

There are intrinsic limitations to the current study. First, an incomplete understanding of the molecular basis of SDD formation makes it impossible to determine the exact reaction equations' parameters at the current time.[3] Ideally, a more biologically specific formula would be specified, such as Michaelis-Menten equations. However, the substrates of the proposed reaction-diffusion system are unknown, and thus we have chosen to present the most general form of the equations driving Turing pattern formation. Second, a criticism of Turing pattern modeling in biological organisms is that they form over a narrow range of reaction parameters. In skin patterning, this criticism may be countered by allowing for evolutionary fine tuning of such parameters as there can be selection pressure associated with skin patterning. Here, however, no known evolutionary advantage is served by having SDD, but fine tuning may still be present as SDDs are only present in the small subset of the adult population (for example, one study found a prevalence of 5.06% in individuals 65 years or older).[29] Third, some studies have suggested that an alternate explanation may be that different patterns of SDD represent different disease processes.[12] However, this is unlikely because multiple patterns have been noted adjacent to each other in the same eye. Importantly, the clinical impact of this finding is still limited, but it may ultimately provide insight into the possible underlying mechanism for SDD formation. It is clinically interesting that the risk ratio of geographic atrophy for each pattern also follows the same order as the Turing pattern spectrum, with risk ratios for neovascular AMD following the opposite direction.[4] The significance of this finding is worthy of further investigation. Finally, whereas this model provides translational relevance by possibly explaining the variation in SDD patterns, in its present state, it does not explain all features of SDD, such as the tendency toward fovea sparing, or increased prevalence in women.[3]

Acknowledgments

Disclosure: **B.K. Young**, None; **L.L. Shen**, Boehringer Ingelheim (C); **L.V. Del Priore**, Boehringer Ingelheim (C); Scientific advisory board - Tissue Regeneration Sciences; LambdaVision, Cavthe Rx; Scientific advisor - Seeing Medicines; Research through university - Stealth Pharmaceuticals

References

1. Spaide RF. Colocalization of pseudodrusen and subretinal drusenoid deposits using high-density en face spectral domain optical coherence tomography. *Retina*. 2014;34:2336–2345.
2. Gliem M, Hendig D, Finger RP, Holz FG, Charbel IP. Reticular Pseudodrusen Associated With a Diseased Bruch Membrane in Pseudoxanthoma Elasticum. *JAMA Ophthalmol*. 2015;133:581–588.
3. Spaide RF, Ooto S, Curcio CA. Subretinal drusenoid deposits AKA pseudodrusen. *Surv Ophthalmol*. 2018;63:782–815.
4. Zhou Q, Daniel E, Maguire MG, et al. Pseudodrusen and Incidence of Late Age-Related Macular Degeneration in Fellow Eyes in the Comparison of Age-Related Macular Degeneration Treatments Trials. *Ophthalmology*. 2016;123:1530–1540.
5. Zweifel SA, Imamura Y, Spaide TC, Fujiwara T, Spaide RF. Prevalence and Significance of Subretinal Drusenoid Deposits (Reticular Pseudodrusen) in Age-Related Macular Degeneration. *Ophthalmology*. 2010;117:1775–1781.
6. Ufret-Vincenty RL, Aredo B, Liu X, et al. Transgenic Mice Expressing Variants of Complement Factor H Develop AMD-like Retinal Findings. *Invest Ophthalmol Vis Sci*. 2010;51:5878–5887.
7. Elfandi S, Ooto S, Ueda-Arakawa N, et al. Clinical and Genetic Characteristics of Japanese Patients with Age-Related Macular Degeneration and Pseudodrusen. *Ophthalmology*. 2016;123:2205–2212.
8. Curcio CA, Messinger JD, Sloan KR, McGwin G, Medeiros NE, Spaide RF. Subretinal drusenoid deposits in non-neovascular age-related macular degeneration: morphology, prevalence, topography, and biogenesis model. *Retina*. 2013;33:265–276.
9. Chen L, Messinger JD, Zhang Y, Spaide RF, Freund KB, Curcio CA. Subretinal drusenoid deposit in age-related macular degeneration: histologic insights into initiation, progression to atrophy, and imaging. *Retina*. 2020;40:618–631.

10. Sohrab MA, Smith RT, Salehi-Had H, Sadda SR, Fawzi AA. Image registration and multimodal imaging of reticular pseudodrusen. *Invest Ophthalmol Vis Sci*. 2011;52:5743–5748.
11. Vongkulsiri S, Ooto S, Mrejen S, Suzuki M, Spaide RF. The lack of concordance between subretinal drusenoid deposits and large choroidal blood vessels. *Am J Ophthalmol*. 2014;158:710–715.
12. Suzuki M, Sato T, Spaide RF. Pseudodrusen subtypes as delineated by multimodal imaging of the fundus. *Am J Ophthalmol*. 2014;157:1005–1012.
13. Turing AM. The chemical basis of morphogenesis. 1953. *Bull Math Biol*. 1990;52:153–197; discussion 119-152.
14. Kondo S, Miura T. Reaction-diffusion model as a framework for understanding biological pattern formation. *Science*. 2010;329:1616–1620.
15. Miyazawa S, Okamoto M, Kondo S. Blending of animal colour patterns by hybridization. *Nature Communications*. 2010;1:66.
16. Mano F, Sprehe N, Olsen TW. Association of Drusen Phenotype in Age-Related Macular Degeneration from Human Eye-Bank Eyes to Disease Stage and Cause of Death. *Ophthalmol Retina*. 2021;8:743–749.
17. Niu S, de Sisternes L, Chen Q, Rubin DL, Leng T. Fully Automated Prediction of Geographic Atrophy Growth Using Quantitative Spectral-Domain Optical Coherence Tomography Biomarkers. *Ophthalmology*. 2016;123:1737–1750.
18. Kamami-Levy C, Querques G, Rostaqui O, Blanco-Garavito R, Souied EH. Choroidal neovascularization associated with extensive macular atrophy with pseudodrusen-like appearance. *Journal Français d'Ophtalmologie*. 2014;37:780–786.
19. Kim JH, Chang YS, Kim JW, Lee TG, Kim CG. Prevalence of subtypes of reticular pseudodrusen in newly diagnosed exudative age-related macular degeneration and polypoidal choroidal vasculopathy in Korean patients. *Retina*. 2015;35:2604–2612.
20. Boyer DS, Schmidt-Erfurth U, van Lookeren Campagne M, Henry EC, Brittain C. The pathophysiology of geographic atrophy secondary to age-related macular degeneration and the complement pathway as a therapeutic target. *Retina (Philadelphia, Pa)*. 2017;37:819.
21. Klein R, Meuer SM, Knudtson MD, Iyengar SK, Klein BE. The epidemiology of retinal reticular drusen. *Am J Ophthalmol*. 2008;145:317–326.
22. Smith RT, Merriam JE, Sohrab MA, et al. Complement Factor H 402H Variant and Reticular Macular Disease. *Arch Ophthalmol*. 2011;129:1061–1066.
23. Ueda-Arakawa N, Ooto S, Nakata I, et al. Prevalence and genomic association of reticular pseudodrusen in age-related macular degeneration. *Am J Ophthalmol*. 2013;155:260–269.e262.
24. Puche N, Blanco-Garavito R, Richard F, et al. Genetic and environmental factors associated with reticular pseudodrusen in age-related macular degeneration. *Retina*. 2013;33:998–1004.
25. Elison JR, Friedman AH, Brodie SE. Acquired subretinal flecks secondary to hypovitaminosis A in a patient with hepatitis C. *Documenta Ophthalmologica*. 2004;109:279–281.
26. Sorsby A, Reading HW, Bunyan J. Effect of Vitamin A Deficiency on the Retina of the Experimental Rabbit. *Nature*. 1966;210:1011–1015.
27. Genead MA, Fishman GA, Lindeman M. Spectral-Domain Optical Coherence Tomography and Fundus Autofluorescence Characteristics in Patients with Fundus Albipunctatus and Retinitis Punctata Albescens. *Ophthalmic Genetics*. 2010;31:66–72.
28. Gliem M, Müller PL, Mangold E, et al. Reticular Pseudodrusen in Sorsby Fundus Dystrophy. *Ophthalmology*. 2015;122:1555–1562.
29. Wilde C, Poostchi A, Mehta RL, et al. Prevalence of reticular pseudodrusen in an elderly UK Caucasian population-The Bridlington Eye Assessment Project (BEAP): a cross-sectional study (2002-2006). *Eye (Lond)*. 2018;32:1130–1137.
30. Chap C. Detail of skin pattern on side of Giant Pufferfish, Tetraodon mbu. 2012, https://upload.wikimedia.org/wikipedia/commons/a/a4/Giant_Pufferfish_skin_pattern_detail.jpg.
31. Häggström M. Medical gallery of Mikael Häggström 2014. *WikiJournal of Medicine*. 2014;1(2):1–55.